Vasily E. Tarasov (Ed.)
Handbook of Fractional Calculus with Applications

Handbook of Fractional Calculus with Applications

Edited by *J. A. Tenreiro Machado*

Volume 1: Theory
Anatoly Kochubei, Yuri Luchko (Eds.), 2019
ISBN 978-3-11-057081-6, e-ISBN (PDF) 978-3-11-057162-2,
e-ISBN (EPUB) 978-3-11-057063-2

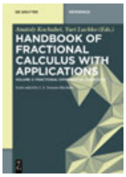

Volume 2: Fractional Differential Equations
Anatoly Kochubei, Yuri Luchko (Eds.), 2019
ISBN 978-3-11-057082-3, e-ISBN (PDF) 978-3-11-057166-0,
e-ISBN (EPUB) 978-3-11-057105-9

Volume 3: Numerical Methods
George Em Karniadakis (Ed.), 2019
ISBN 978-3-11-057083-0, e-ISBN (PDF) 978-3-11-057168-4,
e-ISBN (EPUB) 978-3-11-057106-6

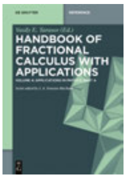

Volume 4: Applications in Physics, Part A
Vasily E. Tarasov (Ed.), 2019
ISBN 978-3-11-057088-5, e-ISBN (PDF) 978-3-11-057170-7,
e-ISBN (EPUB) 978-3-11-057100-4

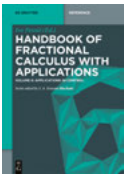

Volume 6: Applications in Control
Ivo Petráš (Ed.), 2019
ISBN 978-3-11-057090-8, e-ISBN (PDF) 978-3-11-057174-5,
e-ISBN (EPUB) 978-3-11-057093-9

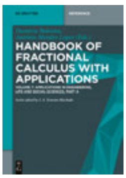

Volume 7: Applications in Engineering, Life and Social Sciences, Part A
Dumitru Băleanu, António Mendes Lopes (Eds.), 2019
ISBN 978-3-11-057091-5, e-ISBN (PDF) 978-3-11-057190-5,
e-ISBN (EPUB) 978-3-11-057096-0

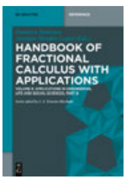

Volume 8: Applications in Engineering, Life and Social Sciences, Part B
Dumitru Băleanu, António Mendes Lopes (Eds.), 2019
ISBN 978-3-11-057092-2, e-ISBN (PDF) 978-3-11-057192-9,
e-ISBN (EPUB) 978-3-11-057107-3

Vasily E. Tarasov (Ed.)

Handbook of Fractional Calculus with Applications

Volume 5: Applications in Physics, Part B

Series edited by Jose Antonio Tenreiro Machado

DE GRUYTER

Editor
Prof. Dr. Vasily E. Tarasov
Lomonosov Moscow State University
Skobeltsyn Inst. of Nuclear Physics
Leninskie Gory
Moscow 119991
Russian Federation
tarasov@theory.sinp.msu.ru

Series Editor
Prof. Dr. Jose Antonio Tenreiro Machado
Department of Electrical Engineering
Instituto Superior de Engenharia do Porto
Instituto Politécnico do Porto
4200-072 Porto
Portugal
jtm@isep.ipp.pt

ISBN 978-3-11-057089-2
e-ISBN (PDF) 978-3-11-057172-1
e-ISBN (EPUB) 978-3-11-057099-1

Library of Congress Control Number: 2018967592

Bibliographic information published by the Deutsche Nationalbibliothek
The Deutsche Nationalbibliothek lists this publication in the Deutsche Nationalbibliografie; detailed bibliographic data are available on the Internet at http://dnb.dnb.de.

Cover image: djmilic / iStock / Getty Images Plus
Typesetting: VTeX UAB, Lithuania
Printing and binding: CPI books GmbH, Leck

www.degruyter.com

Preface

Fractional Calculus (FC) originated in 1695, nearly at the same time as conventional calculus. However, FC attracted a limited attention and remained a pure mathematical exercise in spite of the contributions of important mathematicians, physicists, and engineers. FC had a rapid development during the last few decades, both in mathematics and applied sciences, being nowadays recognized as an excellent tool for describing complex systems, phenomena involving long range memory effects and nonlocality. A huge number of research papers and books devoted to this subject have been published, and presently several specialized conferences and workshops are organized each year. The FC popularity in all fields of science is due to its successful application in mathematical models, namely in the form of FC operators and fractional integral and differential equations. Presently, we are witnessing considerable progress both on theoretical aspects and applications of FC in areas such as physics, engineering, biology, medicine, economy, or finance.

The popularity of FC has attracted many researchers from all over the world and there is a demand for works covering all areas of science in a systematic and rigorous form. In fact, the literature devoted to FC and its applications is huge, but readers are confronted with a high heterogeneity and, in some cases, with misleading and inaccurate information. The Handbook of Fractional Calculus with Applications (HFCA) intends to fill that gap and provides the readers with a solid and systematic treatment of the main aspects and applications of FC. Motivated by these ideas, the editors of the volumes involved a team of internationally recognized experts for a joint publishing project offering a survey of their own and other important results in their fields of research. As a result of these joint efforts, a modern encyclopedia of FC and its applications, reflecting present day scientific knowledge, is now available with the HFCA. This work is distributed by several distinct volumes, each one developed under the supervision of its editors.

The fourth and fifth volumes of HFCA are devoted to the application of fractional calculus (FC) and fractional differential equations in different areas of physics. These volumes describe the fundamental physical effects and, first of all, those that belong to fractional relaxation-oscillation or diffusion-wave phenomena. The FC allows describe spatial nonlocality and fading memory of power-law type, the openness of physical systems and dissipation, long-range interactions, and other physical phenomena. The most well-known physical phenomena and processes, which are described by fractional differential equations, include fractional viscoelasticity, spatial and frequency dispersion of power type, nonexponential relaxation, anomalous diffusion, and many others.

The fifth volume of HFCA focuses on the application of FC in various sections of electrodynamics, statistical physics and physical kinetics, quantum mechanics, and quantum field theory. In the 12 chapters, the most important models with nonlocal-

https://doi.org/10.1515/9783110571721-201

ity, memory of the power type, and openness and dissipation are described in such phenomena as the diffusion-wave, fractional and anomalous diffusion, advection-dispersion, nonexponential relaxation, the spatial and frequency dispersion of power-law type in electrodynamics and quantum mechanics, the openness of quantum systems and dissipation.

My special thanks go to the authors of individual chapters that are excellent surveys of selected classical and new results in several important fields of FC. The editors believe that the HFCA will represent a valuable and reliable reference work for all scholars and professionals willing to develop research in the challenging and timely scientific area.

Vasily E. Tarasov

Contents

Preface —— V

J. A. Tenreiro Machado and António M. Lopes
Fractional electromagnetics —— 1

Vasily E. Tarasov
Fractional electrodynamics with spatial dispersion —— 25

Aleksander Stanislavsky and Karina Weron
Fractional-calculus tools applied to study the nonexponential relaxation in dielectrics —— 53

Yuri Luchko and Francesco Mainardi
Fractional diffusion-wave phenomena —— 71

Rudolf Gorenflo and Francesco Mainardi
Fractional diffusion and parametric subordination —— 99

James F. Kelly and Mark M. Meerschaert
The fractional advection-dispersion equation for contaminant transport —— 129

Vladimir V. Uchaikin and Renat T. Sibatov
Anomalous diffusion in interstellar medium —— 151

Gianni Pagnini
Fractional kinetics in random/complex media —— 183

Nick Laskin
Nonlocal quantum mechanics: fractional calculus approach —— 207

S. C. Lim and Chai Hok Eab
Fractional quantum fields —— 237

Vasily E. Tarasov
Fractional quantum mechanics of open quantum systems —— 257

Alexander Iomin
Fractional quantum mechanics with topological constraint —— 279

Alexander Iomin
Fractional time quantum mechanics —— 299

Index —— 317

J. A. Tenreiro Machado and António M. Lopes

Fractional electromagnetics

Abstract: This chapter addresses the application of fractional calculus (FC) in the area of electromagnetics, and studies four cases, namely the modeling of the electric potential generated by arbitrary charges, electric transmission lines, the skin effect in an electric conductor, and the behavior of a nonlinear electric inductor. The first generalizes the concept of integer to fractional electrostatic multipoles. The second interprets the telegraph equation in the light of FC. The third generalizes the skin effect to inductive effects of any fractional order. The fourth, focuses the modeling of inductors, including phenomena usually overlooked with classical approaches.

Keywords: Fractional calculus, electromagnetics, electric potential, transmission line, skin effect, electric inductor

PACS: 02.30.Jr, 02.60.Cb, 02.70.Bf

1 Introduction

Fractional calculus (FC) generalizes the concepts of classic differential calculus to noninteger orders [36]. During the last decades, FC was adopted for modeling natural and artificial signals and systems characterized by power-law behavior, long range memory effects, nonlocality, and fractal properties [49, 29]. In fact, FC opened new perspectives toward the generalization of classic laws and systems models [34, 41, 28, 7, 25, 6]. In the field of electromagnetics, the tools of FC were applied successfully to describe the behavior of electric machines, transformers, inductors, capacitors, and electronic devices [45, 8, 22, 38, 34, 47, 48].

This chapter addresses the application of FC for modeling several electromagnetic phenomena.

Having these ideas in mind, this chapter is organized as follows. Section 2 models the potential generated by electric charges. Section 3 studies the electric transmission lines. Section 4 addresses the skin effect (SE) in an electric conductor. Section 5 models a nonlinear electric inductor. Finally, Section 6 draws the main conclusions.

J. A. Tenreiro Machado, Institute of Engineering, Polytechnic of Porto, Dept. of Electrical Engineering, Rua Dr. António Bernardino de Almeida, 431, 4249-015 Porto, Portugal, e-mail: jtm@isep.ipp.pt
António M. Lopes, UISPA–LAETA/INEGI, Faculty of Engineering, University of Porto, Rua Dr. Roberto Frias, 4200-465 Porto, Portugal, e-mail: aml@fe.up.pt

https://doi.org/10.1515/9783110571721-001

2 Fractional order potential

Several well-known expressions for the electric potential are related through integer-order integrals and derivatives. Some researchers proposed their generalization based on the concept of fractional-order (FO) poles [23, 15, 42]. This section focuses on the analysis and synthesis of FO multipoles.

For homogeneous, linear, and isotropic media, the electric potential φ at a point P generated by different punctual charge configurations, namely a single charge, a dipole, and a quadrupole, is given by [3]:

$$\varphi = \frac{q}{4\pi\varepsilon_0}\frac{1}{r} + \varphi_0, \tag{1a}$$

$$\varphi = \frac{ql\cos\theta}{4\pi\varepsilon_0}\frac{1}{r^2} + \varphi_0, \quad r \gg l, \tag{1b}$$

$$\varphi = \frac{ql^2(3\cos^2\theta - 1)}{4\pi\varepsilon_0}\frac{1}{r^3} + \varphi_0, \quad r \gg l, \tag{1c}$$

where $\varphi_0 \in \mathbb{R}$ is a constant, ε_0 represents the permittivity, q is the electric charge, r and θ denote the radial distance and the corresponding angle with the axis, and l is the distance between the charges. Therefore, the relationship $\varphi \sim \{r^{-1}, r^{-2}, r^{-3}\}$ results.

For one long straight filament, two filaments with opposite charges and three filaments, carrying the charge λ per unit length, the potential is given by

$$\varphi = -\frac{\lambda}{2\pi\varepsilon_0}\ln r + \varphi_0, \tag{2a}$$

$$\varphi = \frac{\lambda l\cos\theta}{2\pi\varepsilon_0}\frac{1}{r} + \varphi_0, \quad r \gg l, \tag{2b}$$

$$\varphi = \frac{\lambda l^2(\cos^2\theta - 1)}{2\pi\varepsilon_0}\frac{1}{r^2} + \varphi_0, \quad r \gg l, \tag{2c}$$

and the relationship $\varphi \sim \{\ln r, r^{-1}, r^{-2}\}$ applies.

From (1)–(2), we conclude that the expressions for φ are related by integer-order derivatives and integrals.

A FO multipole produces at point P a fractional potential $\varphi \sim r^{\alpha}$, $\alpha \in \mathbb{R}$, meaning that the relationship between φ and r is not restricted to the integer-order integro-differential operator.

Let us consider the potential produced at a point $P = (x, y)$ by a straight filament with finite length l and charge q:

$$\varphi = \frac{1}{4\pi\varepsilon_0}\frac{q}{l}\ln\left[\frac{y + \frac{1}{2}l + \sqrt{x^2 + (y + \frac{1}{2}l)^2}}{y - \frac{1}{2}l + \sqrt{x^2 + (y - \frac{1}{2}l)^2}}\right] + \varphi_0. \tag{3}$$

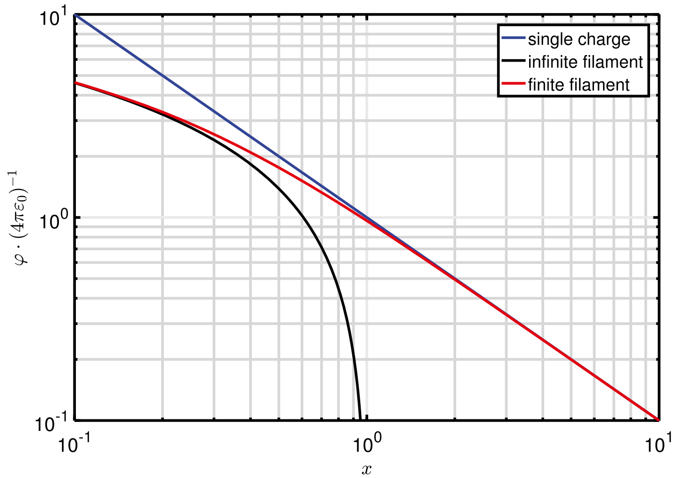

Figure 1: The potential φ of formula (3) versus x, for $y = 0$, and the two limits given by (1a) and (2a), for $q = 1$, $l = 1$, and $\varphi_0 = 0$.

For $y = 0$ and $x \to \infty$, the asymptotic expansion of the potential is $\varphi \to \frac{q}{4\pi\varepsilon_0}\frac{1}{x} + \varphi_0$, while for $y = 0$ and $x \to 0$ yields $\varphi \to \frac{1}{2\pi\varepsilon_0}\frac{q}{l}\ln(\frac{1}{x}) + \varphi_0$. These limits correspond to (1a) and (2a), that is, to the electric potentials produced by a single charge and by an infinite filament, respectively. Figure 1 depicts the potential (3) versus x and, for comparison, the two limits given by (1a) and (2a), for $q = 1$, $l = 1$ and $\varphi_0 = 0$.

We verify that expression (3) represents a potential changing smoothly between the two limit cases, leading to the conclusion that an intermediate FO relationship is possible, at least within a limited working range. Figure 2 shows the approximations $\varphi_A \approx 1.385x^{-0.532}$, within the interval $x \in [0.1, 0.3]$, and $\varphi_A \approx 1.031x^{-0.747}$, within $x \in [0.3, 0.8]$, for $y = 0$, $q = 1$, $l = 1$, and $\varphi_0 = 0$. We conclude that the standard integer-order potential relationships have a “global” nature, while FO potentials have a “local” nature, possible to capture only in a restricted interval of space.

In the follow-up, a numerical algorithm for generating a given FO potential is presented [38, 23].

The method fits the nth order approximation, $\varphi_A^n(x)$, based on single charges, to a reference model, $\varphi_R(x)$, while minimizing the optimization index, J [9]:

$$\varphi_A^n(x) = \sum_{i=1}^{n} \frac{1}{4\pi\varepsilon_0}\frac{q_i}{|x - x_i|}, \quad q_i, x_i \in \mathbb{R}, \tag{4}$$

$$\varphi_R(x) = mr^{\alpha}, \quad m, \alpha \in \mathbb{R}, \tag{5}$$

$$J = \frac{1}{K}\sum_{k=1}^{K} \frac{|\varphi_A^n(x_k) - \varphi_R(x_k)|}{|\varphi_A^n(x_k)| + |\varphi_R(x_k)|}, \quad x_k \in [x_a, x_b], \tag{6}$$

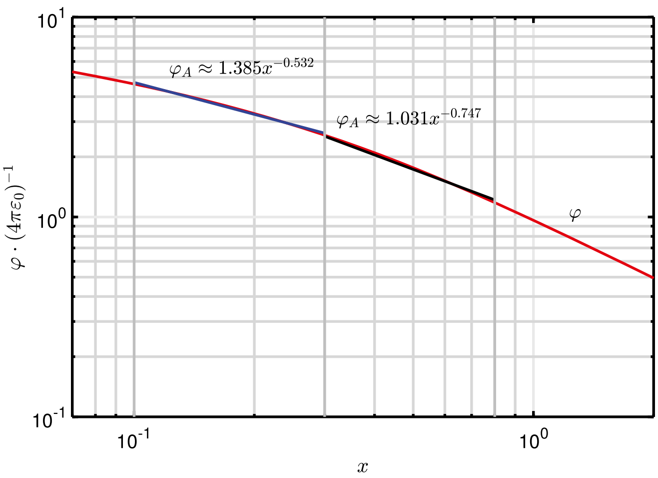

Figure 2: Approximations of the potential φ of formula (3), for $y = 0$, $q = 1$, $l = 1$, and $\varphi_0 = 0$, with $\varphi_A \approx 1.385x^{-0.532}$ and $\varphi_A \approx 1.031x^{-0.747}$, within the intervals $x \in [0.1, 0.3]$ and $x \in [0.3, 0.8]$, respectively.

where K represents the number of points in $x_k \in [x_a, x_b]$, q_i denotes electrical charges, x_i represents the ith charge position, m is a constant, and α is the FO. This means that the algorithm places n charges q_i, $i = 1, 2, \ldots, n$, at the positions x_i, so that $\varphi_A^n \approx mr^\alpha$, within the interval $x \in [x_a, x_b]$.

For example, Figure 3 shows the $n = 4$ charge approximations to the reference potentials of $\varphi_R = 1.5x^{-0.6}$ and $\varphi_R = 1.5x^{-1.3}$ for $K = 400$ points linearly spaced within the interval $x \in [1, 3]$. The charges and positions are $q_i = \{3.09 \times 10^{-5}, -6.59, 8.22, -0.99\}$ and $x_i = \{3.39, 0.21, 0.19, -1.79\}$, and $q_i = \{6.05, 0.01, 1.22, 0.94\}$ and $x_i = \{-23.75, 0.50, -1.95, -0.13\}$, respectively.

The results show a good fit between φ_A^n ($n = 4$) and φ_R. Nevertheless, for a given application, a superior precision may be required and, in that case, a larger number of charges must be used. Table 1 shows the values of J obtained for the n-charge approximations, $n = 1, \ldots, 10$, of $\varphi_R = 1.5x^{-1.6}$, $\varphi_R = 1.5x^{-1.4}$, $\varphi_R = 1.5x^{-0.6}$, and $\varphi_R = 1.5x^{-0.4}$, with $K = 400$ points linearly spaced within the interval $x \in [1, 3]$. Figure 4 depicts the $\{n, J\}$ locus. We verify that J diminishes as n increases, yielding a better approximation of φ_A^n to φ_R.

3 Fractional-order modeling of transmission lines

During the twentieth century, electric power transmission, telecommunications, and microwave engineering made popular the theory of transmission lines [10, 2]. In this section, the transmission lines are reviewed at light of FC [35].

Table 1: Values of J for the n-charge approximations, $n = 1, \dots, 10$, of $\varphi_R = 1.5x^{-1.6}$, $\varphi_R = 1.5x^{-1.4}$, $\varphi_R = 1.5x^{-0.6}$, and $\varphi_R = 1.5x^{-0.4}$, within the interval $x \in [1, 3]$.

n	**1**	**2**	**3**	**4**	**5**	**6**	**7**	**8**	**9**	**10**
$\varphi_R = 1.5x^{-1.6}$										
J ($\times 10^{-7}$)	224934.4	500.5	343.7	297.1	272.9	268.5	234.7	127.0	83.9	54.3
$\varphi_R = 1.5x^{-1.4}$										
J ($\times 10^{-7}$)	127162.8	703.7	550.3	387.4	269.1	262.1	150.0	136.1	54.1	36.6
$\varphi_R = 1.5x^{-0.6}$										
J ($\times 10^{-7}$)	47473.3	225.4	21.5	5.8	4.5	3.7	2.1	1.2	1.1	0.6
$\varphi_R = 1.5x^{-0.4}$										
J ($\times 10^{-7}$)	46010.6	219.9	26.7	13.3	4.1	1.6	1.0	0.8	0.2	0.2

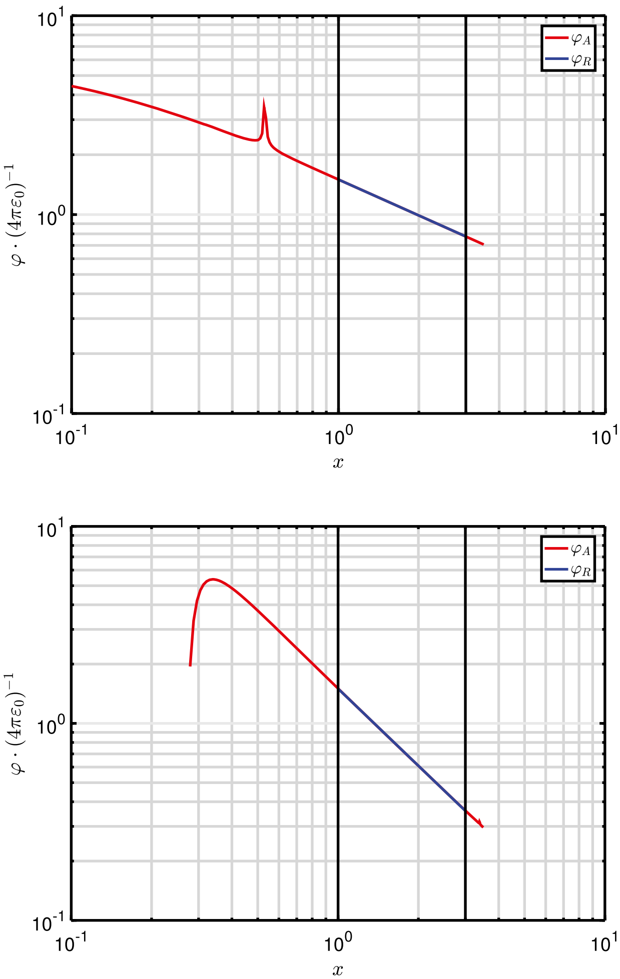

Figure 3: The $n = 4$ charge approximations of $\varphi_R = 1.5x^{-0.6}$ and $\varphi_R = 1.5x^{-1.3}$ for $K = 400$ points linearly spaced within the interval $x \in [1, 3]$.

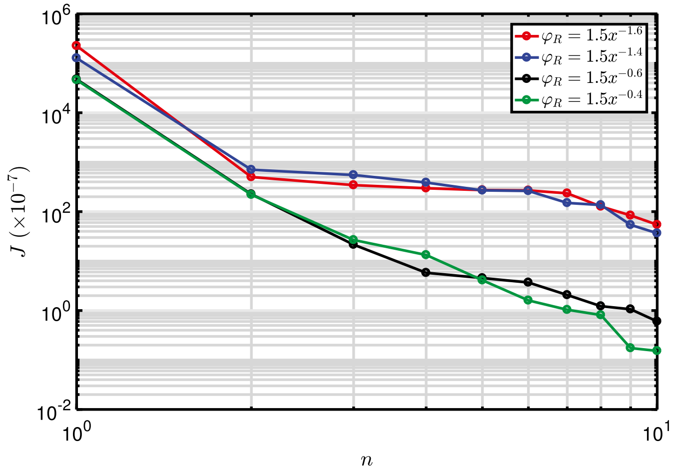

Figure 4: The relationship between J and n for $\varphi_R = 1.5x^{-1.6}$, $\varphi_R = 1.5x^{-1.4}$, $\varphi_R = 1.5x^{-0.6}$, and $\varphi_R = 1.5x^{-0.4}$, within the interval $x \in [1, 3]$.

The model of a uniform transmission line is derived by considering an infinitesimal length dx located at coordinate x. The model is also called telegrapher's equations and the values of the components are specified per unit length. Therefore, we have four parameters:

- distributed resistance R of the conductors, represented in series (with units Ohm per unit length).
- distributed self-inductance L, represented in series (expressed in Henry per unit length).
- distributed capacitance C between the two conductors, modeled by a shunt capacitor (in Farad per unit length).
- distributed conductance G of the dielectric material separating the two conductors, described by a shunt resistor (in Siemens per unit length).

The line segment has series resistance and inductance Rdx and Ldx, and shunt conductance and capacitance Gdx and Cdx, respectively (see the diagram of Figure 5, where t represents time, and v and i denote the electrical voltage and current).

The application of the Kirchoff's laws to the circuit leads to the set of partial differential equations:

$$\frac{\partial v(x,t)}{\partial x} = -L\frac{\partial i(x,t)}{\partial t} - Ri(x,t), \tag{7a}$$

$$\frac{\partial i(x,t)}{\partial x} = -C\frac{\partial v(x,t)}{\partial t} - Gv(x,t). \tag{7b}$$

Some additional calculations allow the elimination of one variable and to write the differential equation either with respect to v or to i, yielding

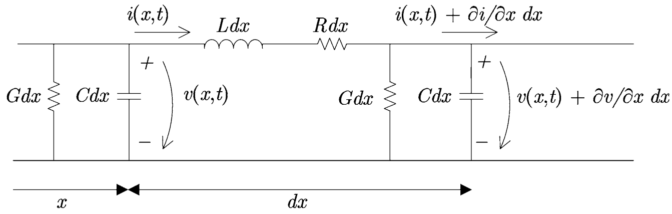

Figure 5: Electrical circuit of an infinitesimal portion of a uniform transmission line.

$$\frac{\partial^2 v(x,t)}{\partial x^2} = LC\frac{\partial^2 v(x,t)}{\partial t^2} + (LG + RC)\frac{\partial v(x,t)}{\partial t} + RGv(x,t), \tag{8}$$

or

$$\frac{\partial^2 i(x,t)}{\partial x^2} = LC\frac{\partial^2 i(x,t)}{\partial t^2} + (LG + RC)\frac{\partial i(x,t)}{\partial t} + RGi(x,t). \tag{9}$$

When $L = 0$ and $G = 0$, equations (8)–(9) reduce to the equivalent of the heat diffusion equation, where v and i are the analogs of the temperature and the heat flux, respectively.

To analyze the transmission line in the frequency domain, the Fourier transform operator $\mathcal{F}$ is applied to equation (7), yielding

$$\frac{dV(x,j\omega)}{dx} = -Z(j\omega)I(x,j\omega), \tag{10a}$$
$$\frac{dI(x,j\omega)}{dx} = -Y(j\omega)V(x,j\omega), \tag{10b}$$

where ω is the angular frequency, $j = \sqrt{-1}$, $I(x,j\omega) = \mathcal{F}\{i(x,t)\}$, $V(x,j\omega) = \mathcal{F}\{v(x,t)\}$, $Z(j\omega) = R + j\omega L$, and $Y(j\omega) = G + j\omega C$. In the same line of thought, equation (8) is transformed to

$$\frac{d^2 V(x,j\omega)}{dx^2} = -Z(j\omega)Y(j\omega)V(x,j\omega). \tag{11}$$

Equation (11) has solution in the frequency domain given by

$$V(x,j\omega) = A_1 e^{\gamma x} + A_2 e^{-\gamma x}, \tag{12a}$$
$$I(x,j\omega) = Z_c^{-1}(A_2 e^{-\gamma x} - A_1 e^{\gamma x}), \tag{12b}$$

where

$$Z_c(j\omega) = \sqrt{Z(j\omega)Y^{-1}(j\omega)} = \sqrt{(R + j\omega L)/(G + j\omega C)}, \tag{13}$$

is called characteristic impedance, and

$$\gamma(j\omega) = \sqrt{Z(j\omega)Y(j\omega)} = \alpha(\omega) + j\beta(\omega). \tag{14}$$

These expressions have two terms corresponding to waves traveling in opposite directions: the term proportional to $e^{-\gamma x}$ is due to the signal applied at the line input, while the term $e^{\gamma x}$ represents the reflected wave.

For a transmission line of length l, it is usual to adopt for variable the distance up to the end given by

$$x' = l - x. \tag{15}$$

If V_2 and I_2 represent the voltage and current at the end of the transmission line, then the Fourier transforms of equation (7) at coordinate x' are given by

$$V(x, j\omega) = V_2 \cosh(\gamma x') + I_2 Z_c \sinh(\gamma x'), \tag{16a}$$

$$I(x, j\omega) = V_2 Z_c^{-1} \sinh(\gamma x') + I_2 \cosh(\gamma x'). \tag{16b}$$

For a loading impedance $Z_2(j\omega)$, it results in $V_2(j\omega) = Z_2(j\omega) I_2(j\omega)$ and the input impedance $Z_i(j\omega)$ of the transmission line is given by

$$Z_i(x, j\omega) = [Z_2 \cosh(\gamma x') + Z_c \sinh(\gamma x')] \cdot [Z_2 Z_c^{-1} \sinh(\gamma x') + \cosh(\gamma x')]^{-1}. \tag{17}$$

Typically, at the end of the line three cases are considered: namely, short circuit, open circuit, and adapted line. These conditions simplify equation (17), yielding

$$\text{short circuit:} \quad V_2 = 0, Z_2(j\omega) = 0 \Rightarrow Z_i(j\omega) = Z_c(j\omega) \tanh(\gamma l), \tag{18a}$$

$$\text{open circuit:} \quad I_2 = 0, Z_2(j\omega) = \infty \Rightarrow Z_i(j\omega) = Z_c(j\omega) \coth(\gamma l), \tag{18b}$$

$$\text{adapted line:} \quad Z_2(j\omega) = Z_c(j\omega) \Rightarrow Z_i(j\omega) = Z_c(j\omega). \tag{18c}$$

The classic perspective is to study lossless lines (i. e., $R = 0$ and $G = 0$). This approach is reasonable in real-world power systems, and models in the frequency domain lead to two-port networks usually analyzed under the light of integer order elements. Nevertheless, the transcendental equations (17) and (18) yield both to integer and FO expressions. For example, in the case of an adapted line (with $R, C, L, G \in \mathbb{R}^+$), we can have half-order FO capacitances and half-order FO inductances, accordingly with the expressions:

$$L = 0, G = 0 \Rightarrow Z_c(j\omega) = \sqrt{(j\omega)^{-1} R C^{-1}}, \tag{19a}$$

$$R = kL, G = kC \Rightarrow Z_c(j\omega) = \sqrt{R L^{-1}}, \tag{19b}$$

$$R = 0, C = 0 \Rightarrow Z_c(j\omega) = \sqrt{j\omega L G^{-1}}, \tag{19c}$$

where $k \in \mathbb{R}^+$.

Since conditions (18a) and (18b) are easier to implement in practice than (18c), we follow the asymptotic expansions of $\tanh(\gamma l)$ and $\coth(\gamma l)$. Knowing that for low frequencies we have $\omega \to 0$, $\tanh(\gamma l) \to \gamma l$, $\coth(\gamma l) \to (\gamma l)^{-1}$, and that for high frequencies $\omega \to \infty$, $\tanh(\gamma l) \to 1$, $\coth(\gamma l) \to 1$, we obtain approximations for the short and open circuit cases, given by

$$Z_i(j\omega) = \begin{cases} Z(j\omega)l, & \omega \to 0, \\ Z_c(j\omega), & \omega \to \infty, \end{cases} \tag{20a}$$

$$Z_i(j\omega) = \begin{cases} [Y(j\omega)l]^{-1}, & \omega \to 0, \\ Z_c(j\omega), & \omega \to \infty. \end{cases} \tag{20b}$$

We conclude that both cases approximate the condition (18c) when $\omega \to \infty$.

These results are overlooked in the textbooks and suggest possible strategies for implementing FO impedances. Hardware strategies for implementing FO derivatives have been pointed out in order to avoid computational approximation schemes [51]. Therefore, it is relevant to explore fractal geometries and dielectric properties [46, 5] to achieve FO capacitors and inductors.

4 Fractional-order skin effect

The effect of a high-frequency electric current to distribute itself in a conductor so that the current density near the surface is higher than that at its core is called SE. This phenomenon reveals characteristics well modeled by the FC tools, exhibiting a dynamics of half-order. Moreover, the model development based on the Maxwell's equations suggests the implementation of inductive devices of FO [39, 4, 8, 44, 37].

Let us denote by ∇ the nabla operator. In the differential form, the Maxwell equations are given by [27]:

$$\nabla \times \mathbf{E} = -\frac{\partial \mathbf{B}}{\partial t}, \tag{21}$$

$$\nabla \times \mathbf{H} = \mathbf{J} + \frac{\partial \mathbf{D}}{\partial t}, \tag{22}$$

$$\nabla \cdot \mathbf{D} = \rho, \tag{23}$$

$$\nabla \cdot \mathbf{B} = 0, \tag{24}$$

where $\mathbf{E}$, $\mathbf{D}$, $\mathbf{H}$, $\mathbf{B}$, $\mathbf{J}$ represent the vectors of electric field intensity, electric flux density (or electric displacement), magnetic field intensity, magnetic flux density and the current density, respectively, and ρ is the charge density.

For homogeneous, linear, and isotropic media, we write

$$\mathbf{D} = \varepsilon \mathbf{E}, \tag{25}$$

$$\mathbf{B} = \mu \mathbf{H}, \tag{26}$$

$$\mathbf{J} = \gamma \mathbf{E}, \tag{27}$$

where ε, μ, and γ are the electrical permittivity, the magnetic permeability, and the conductivity, respectively.

We consider a cylindrical conductor with radius r_0 conducting a current I along its longitudinal axis. In a conductor, even for high frequencies, the term $\frac{\partial \mathbf{D}}{\partial t}$ is negligible in comparison with the conduction term $\mathbf{J}$, that is, the displacement current is much lower than the conduction current, and equation (22) simplifies to $\nabla \times \mathbf{H} = \mathbf{J}$. Therefore, for a radial distance $r < r_0$ the application of the Maxwell's equations with the simplification of (22) leads to the expression [26, 3]:

$$\nabla \times (\nabla \times \mathbf{J}) = -\gamma\mu \frac{\partial \mathbf{J}}{\partial t}. \tag{28}$$

Knowing that $\nabla \times (\nabla \times \mathbf{J}) = \nabla(\nabla \cdot \mathbf{J}) - \nabla^2 \mathbf{J}$, where ∇^2 is the Laplacian, and that $\nabla \cdot \mathbf{J} = 0$, it results in

$$\nabla^2 \mathbf{J} = \gamma\mu \frac{\partial \mathbf{J}}{\partial t}. \tag{29}$$

For cylindrical coordinates and for $\mathbf{J}$ pointing in the direction of the z axis, the Laplacian can be expressed as $\nabla^2 \mathbf{J} = \frac{1}{r}\frac{\partial}{\partial r}(r \frac{\partial \mathbf{J}}{\partial t})$. Therefore, rewriting (29) in terms of the electric field intensity E, it comes as

$$\frac{\partial^2 E}{\partial r^2} + \frac{1}{r}\frac{\partial E}{\partial r} = \gamma\mu \frac{\partial E}{\partial t}. \tag{30}$$

For a sinusoidal field $E \sin(\omega t)$, we adopt the complex notation $Ee^{j\omega t}$, yielding

$$\frac{d^2 E}{dr^2} + \frac{1}{r}\frac{dE}{dr} + q^2 E = 0, \tag{31}$$

with $v^2 = -j\omega\gamma\mu$.

Equation (31) is a particular case of the Bessel equation that has a solution:

$$E(r) = \frac{v}{2\pi r_0 \gamma} \frac{J_0(vr)}{J_1(vr_0)} I, \quad 0 \le r \le r_0, \tag{32}$$

where $J_0(\cdot)$ and $J_1(\cdot)$ are complex valued Bessel functions of the first kind of orders 0 and 1, respectively.

Equation (32) characterizes the SE phenomenon consisting of a nonuniform current density, namely a low density near the conductor axis and a high density on surface, the higher the frequency ω. Therefore, for a conductor of length l_0 the total voltage drop is $ZI = E(r = r_0)l_0$ and the equivalent electrical complex impedance Z is given by

$$Z = \frac{q l_0}{2\pi r_0 \gamma} \frac{J_0(vr)}{J_1(vr_0)}. \tag{33}$$

For small values of x, the Taylor series [43] leads to

$$J_0(x) = 1 - \frac{x^2}{2^2} + \cdots, \tag{34}$$

$$J_1(x) = \frac{x}{2} - \frac{x^3}{2^2 4} + \cdots, \tag{35}$$

while for large values of x the asymptotic expansion yields

$$J_n(x) = \sqrt{\frac{2}{\pi x}} \cos\left(x - n\frac{\pi}{2} - \frac{\pi}{4}\right), \quad n = 0, 1, \ldots. \tag{36}$$

Knowing the expansions (34), (35), and (36), the low and high frequency approximations of Z can be written as

$$\omega \to 0 \Rightarrow Z \to \frac{l_0}{\pi r_0^2 \gamma}, \tag{37}$$

$$\omega \to \infty \Rightarrow Z \to \frac{l_0}{2\pi r_0} \sqrt{\frac{\omega\mu}{2\gamma}} (1 + j). \tag{38}$$

The standard approach to avoid handling the transcendental equation (33) is to approximate Z by means of a resistance R_a and an inductance L_a given by $Z = R_a + j\omega L_a$. Nevertheless, this method is inadequate because the model parameters $\{R_a, L_a\}$ must vary with the frequency (see Figure 6).

Expression (38) reveals the half-order nature of the dynamic phenomenon, at high frequencies (i. e., $Z \sim \omega^{\frac{1}{2}}$) which is not captured by the classic integer-order modeling.

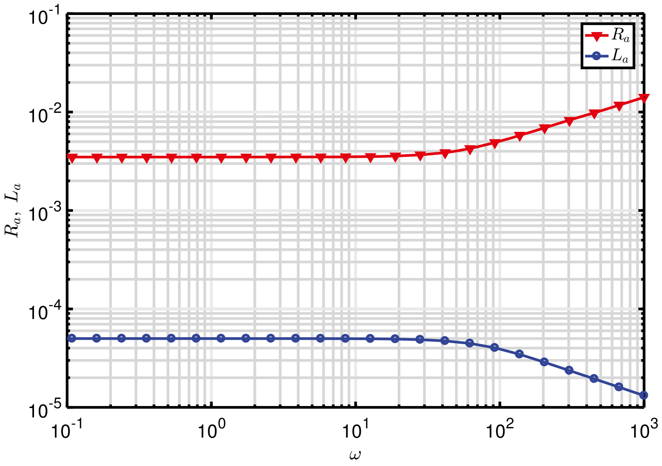

Figure 6: Variation of R_a and L_a for the integer order model $Z = R_a + j\omega L_a$ with $\gamma = 10^7\ \Omega^{-1}$m, $l_0 = 1$ m, $r_0 = 3.02 \cdot 10^{-3}$ m, $\mu_0 = 1.257 \cdot 10^{-6}$ Hm^{-1}, and $\mu_r = 10^3$.

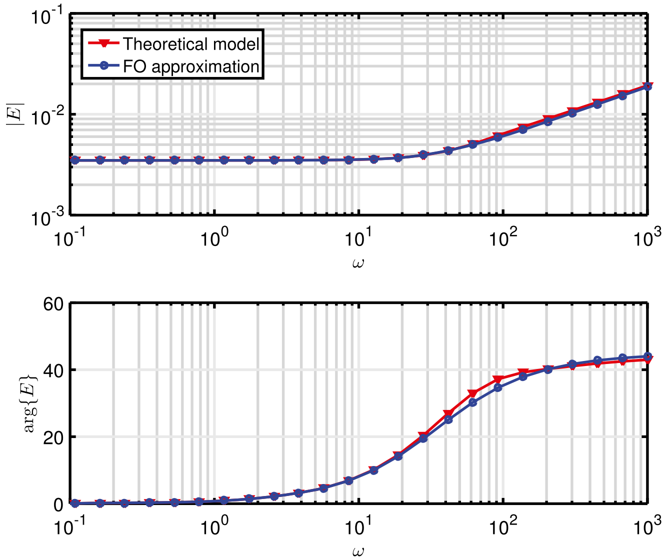

Figure 7: Amplitude and phase Bode diagrams of the electrical field at $r = r_0$, $E(r_0)$, for the theoretical and the approximate expression (39) with $\gamma = 10^7\ \Omega^{-1}$m, $l_0 = 1$ m, $r_0 = 3.02 \cdot 10^{-3}$ m, $\mu_0 = 1.257 \cdot 10^{-6}$ Hm^{-1}, and $\mu_r = 10^3$.

The FC eliminates that limitation [35, 39]. A simple method is to join the two asymptotic expressions (37)–(38) by means of the FO reference (approximation) model:

$$Z_R = Z_0 \left(1 + \frac{j\omega}{z}\right)^{\alpha}, \tag{39}$$

where $Z_0 = \frac{l_0}{\pi r_0^2 \gamma}$, $z = \frac{4}{r_0^2 \gamma \mu}$, and $\alpha = \frac{1}{2}$.

Figure 7 compares the Bode diagrams of amplitude and phase of $E(r_0)$ based on expressions (33) and (39) in the case of a conductor with $\gamma = 10^7\ \Omega^{-1}$m, $l_0 = 1$ m, $r_0 = 3.02 \cdot 10^{-3}$ m, $\mu_0 = 1.257 \cdot 10^{-6}$ Hm^{-1}, and $\mu_r = 10^3$. We verify that (39) leads to a very good curve fitting.

Other values of α can be designed, either by varying the geometry of the conductor, or by modifying its electromagnetic properties.

Equation (31) is now integrated numerically adopting the Euler forward approximation for the first- and second-order derivatives of the sinusoidal electric field, E. We get the approximate

$$E(k+2) + \left(-2 + \frac{\Delta r}{r}\right) E(k+1) + \left(1 - \frac{\Delta r}{r}\right) E(k) - j\omega\mu\Delta r^2 \gamma(r) E(k) = 0, \tag{40}$$

where k and $k + 1$ represent two consecutive sampling points in space and Δr is the integration step along the conductor radius.

The numerical initialization must be obtained from the boundary conditions:

$$H = \frac{1}{j\omega\mu}\frac{dE}{dr}, \tag{41}$$

$$H_0 = H(r = r_0) = \frac{I}{2\pi r_0}. \tag{42}$$

The calculation of (40) requires initial conditions compatible with (41)–(42). The initial conditions are estimated by means of a Genetic Algorithm (GA) [40], with population $\{\mathbb{R}\{E(1)\}, \mathbb{R}\{E(0)\}, \mathbb{J}\{E(1)\}, \mathbb{J}\{E(0)\}\}$, and fitness function

$$J_{\text{init}} = \left[\frac{1}{\omega\mu}\frac{\mathbb{J}\{E(k+1)\} - \mathbb{J}\{E(k)\}}{\Delta r}\right]^2 + \left[\mathbb{R}\{E(k+1)\} - \mathbb{R}\{E(k)\}\right]^2, \tag{43}$$

$$H_0 = \frac{1}{\omega\mu}\frac{\mathbb{J}\{E(k_0)\} - \mathbb{J}\{E(k_0-1)\}}{\Delta r}, \tag{44}$$

where $k_0\Delta r = r_0$. It adopted a GA population of 2000 elements, crossover and mutation probabilities of $p_c = 0.5$ and $p_m = 0.1$, respectively, and elitism. Furthermore, the GA was executed during $n_{\text{GA}} = 2000$ iterations for a total of K testing frequencies, logarithmically spaced in the interval $\omega_{\min} < \omega < \omega_{\max}$, of the sinusoidal electric field E. In the numerical experiments a set of frequencies Ω was considered such that $\omega_{\min} = 10^{-2}$, $\omega_{\max} = 10^3$ and $K = 30$.

Expressions (43)–(44) pose a considerable computational load, for the initialization GA. In order to reduce the burden the integration step Δr was adjusted, from gross to fine, during three phases in the GA evolution, namely

$$\Delta r(n) = \begin{cases} \frac{r_0}{66} & n \le \frac{1}{3}n_{\text{GA}}, \\ \frac{r_0}{133} & \frac{1}{3}n_{\text{GA}} < n \le \frac{2}{3}n_{\text{GA}}, \\ \frac{r_0}{200} & \frac{2}{3}n_{\text{GA}} < n \le n_{\text{GA}}, \end{cases} \tag{45}$$

where the index n represents the GA iterations.

This algorithm guarantees the convergence of the numerical integration of (40) and leads to a reduction of 50 % in the computational burden of the fitness evaluation. In fact, several experiments, comparing the results of the variable and the fixed step sizes, demonstrated the feasibility of the proposed scheme.

The first approach for modifying the properties of the SE consists of adopting a conductor with a different geometry. One simple possibility is, for example, to have a annular conductor with inner and outer radius r_1 and r_0, respectively. Figure 8 shows the amplitude and phase Bode diagrams of the electrical field at $r = r_0$, $E(k_0)$, for $r_1 = \{0, 0.3, 0.5, 0.7\} \cdot r_0$. We verify that by eliminating the flow of current in the inner part of the conductor we can shift the frequency response.

The second approach for a different SE consists of varying the electrical conductivity with the conductor radial distance, that is, to have $\gamma = \gamma(r)$, $r_1 \le r \le r_0$. For the

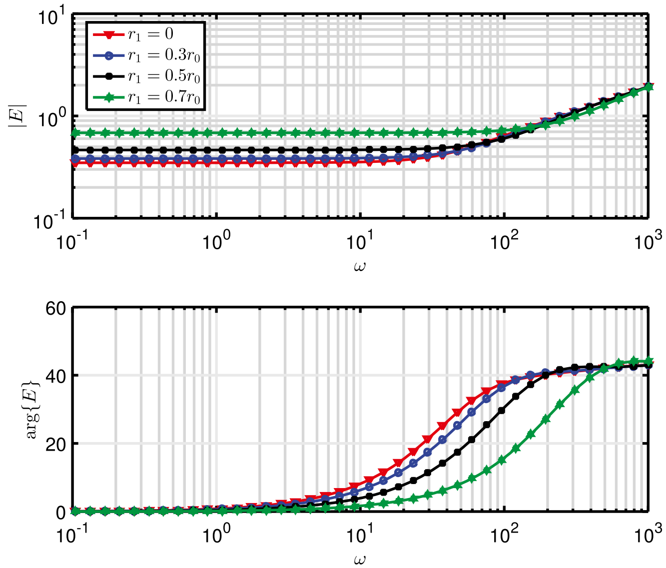

Figure 8: Amplitude and phase Bode diagrams of the electrical field at $r = r_0$, $E(r_0)$, for a annular conductor with inner and outer radius r_1 and r_0, such that $r_1 = \{0, 0.3, 0.5, 0.7\} \cdot r_0$, with $\gamma = 10^7\ \Omega^{-1}\mathrm{m}$, $l_0 = 1\,\mathrm{m}$, $r_0 = 3.02 \cdot 10^{-3}$ m, $\mu_0 = 1.257 \cdot 10^{-6}\ \mathrm{Hm}^{-1}$, and $\mu_r = 10^3$.

electrical conductivity, the following expression was considered:

$$\gamma(r) = \gamma_0 \left(1 - \frac{r - r_1}{r_0}\right)^{\beta}, \quad -\infty < \beta < +\infty, \tag{46}$$

Obviously, $\beta = 0$ yields the case of constant electrical conductivity that was analyzed above.

During the experiments the numerical values $\gamma = 10^7\ \Omega^{-1}\mathrm{m}$, $r_0 = 3.02 \cdot 10^{-3}$ m, $\mu_0 = 1.257 \cdot 10^{-6}\ \mathrm{Hm}^{-1}$, $\mu_r = 10^3$, $\omega_{\min} = 10^{-2}\ \mathrm{s}^{-1}$, and $\omega_{\max} = 10^3\ \mathrm{s}^{-1}$ were adopted.

Figure 9 depicts the Bode diagrams of amplitude and phase of $E(k_0)$ for $\beta = \{-1, -\frac{1}{2}, 0, \frac{1}{2}, 1\}$.

It was observed that when moving far away from the central case of $\beta = 0$ the results became more and more "unstable," that is, with considerable variations in the plots. Therefore, in the study were considered only those cases that depicted a sound numerical response.

The Bode plots reveal that at low frequencies we get the usual resistive behavior, but at high frequencies we have inductive effects of different FO. Therefore, it was decided to approximate the numerical results by a reference expression:

$$E_R = E_0 \left(1 + \frac{j\omega}{z}\right)^{\alpha}, \quad E_0 > 0,\ z > 0,\ \alpha > 0, \tag{47}$$

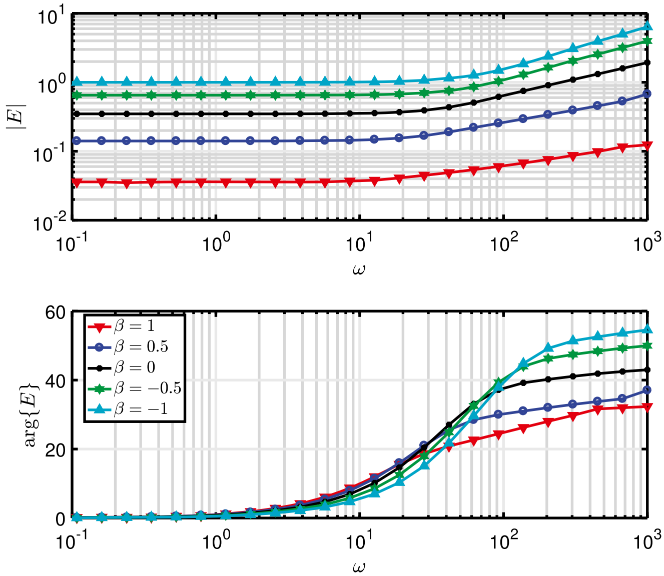

Figure 9: Amplitude and phase Bode diagrams of the electrical field at $r = r_0$, $E(r_0)$, for $\gamma = 10^7\ \Omega^{-1}\mathrm{m}$, $r_0 = 3.02 \cdot 10^{-3}$ m, $\mu_0 = 1.257 \cdot 10^{-6}\ \mathrm{Hm}^{-1}$, $\mu_r = 10^3$, and $\beta = \{-1, -\frac{1}{2}, 0, \frac{1}{2}, 1\}$.

For the estimation of the three parameters $\{E_0, z, \alpha\}$, an identification GA with fitness function:

$$J_{\text{ident}} = \sum \left[\Re(E_R) - \Re\{E(k_0)\}\right]^2 + \left[\Im(E_R) - \Im\{E(k_0)\}\right]^2, \tag{48}$$

was implemented, where Ω represents the set of K sampling frequencies such that $\omega_{\min} < \omega < \omega_{\max}$. The parameters of the identification GA are: population of $n_{\text{GA}} = 5000$ elements, crossover and mutation probabilities of $p_c = 0.5$ and $p_m = 0.1$, respectively, and elitism. The GA was executed during 1000 iterations, for $\omega_{\min} = 10^{-2}$, $\omega_{\max} = 10^3$ and $K = 30$.

Figure 10 depicts the parameters $\{E_0, z, \alpha\}$ of expression (47) versus β. We verify clearly that by varying the electrical conductivity in (46) we can design different values of α.

5 Fractional-model of an inductor

An ideal inductor is characterized by the impedance $Z(j\omega) = j\omega L$, where the parameter L denotes the inductance. However, such device has no physical correspondence, since the model ignores the ohmic resistance of the winding, the parasitic capacitance between neighbor turns, the hysteresis and eddy-current losses in the magnetic core,

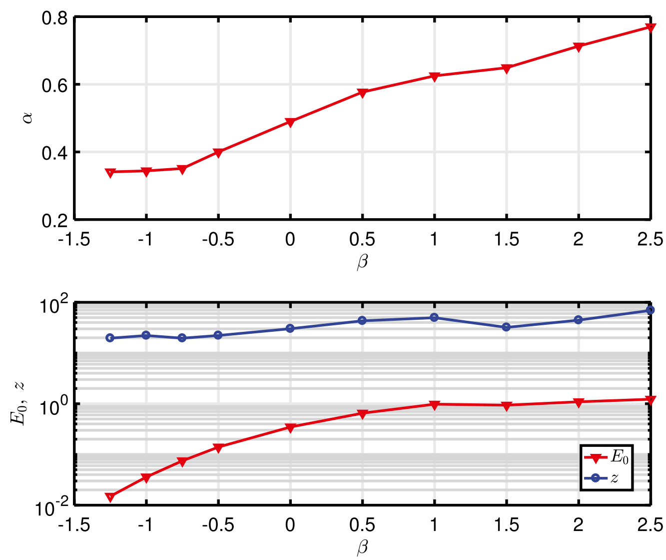

Figure 10: Variation of the parameters $\{E_0, z, \alpha\}$ versus β.

and the SE in the wire. Additionally, the nonlinearities are dependent on the amplitude and frequency, ω, being more critical when ω is high [47].

Classic models represent a real inductor by means of equivalent electric circuits, where the inductor is associated in series/parallel with resistances and capacitors. Nevertheless, these models reveal difficulties in describing the nonlinear and the SE that characterize many inductors, and their accurate modeling is a challenging exercise [48]. In this section, the FC perspective is adopted for describing an inductor [31]. The electrical impedance spectroscopy (EIS) technique is used for measuring the equivalent impedance of the device, and the experimental data is approximated by means of FO empirical transfer functions [11, 12, 20, 21].

The EIS technique measures the electrical impedance of a specimen object [29, 30]. The EIS is straightforward to implement, avoiding complicated procedures and time consuming measurements. The EIS has been used in the description of vegetable [14, 24] and animal [18] tissues, food liquids [32, 33], materials [50, 16], and electrical devices [17, 1].

The EIS starts by applying to the sample electric sinusoidal input signals, and registering the amplitude and phase shift of the output steady-state sinusoidal voltage, $v(t)$, and current, $i(t)$:

$$v(t) = V\cos(\omega t + \theta_V), \tag{49a}$$

$$i(t) = I\cos(\omega t + \theta_I), \tag{49b}$$

where $\{V, I\}$ and $\{\theta_V, \theta_I\}$ are the amplitudes and phase shifts of the voltage and current, respectively.

The signals $v(t)$ and $i(t)$ can be represented in the Fourier domain:

$$V(j\omega) = V \cdot e^{j\theta_V}, \tag{50a}$$

$$I(j\omega) = I \cdot e^{j\theta_I}, \tag{50b}$$

where the impedance $Z(j\omega)$ is given by

$$Z(j\omega) = \frac{V(j\omega)}{I(j\omega)} = \frac{V}{I} \cdot e^{j(\theta_V - \theta_I)} = |Z(j\omega)| \cdot e^{j \arg [Z(j\omega)]}. \tag{51}$$

The diagram of Figure 11 shows the experimental set-up [29, 30] using general purpose equipment. The inductor is connected in series with an adaptation metal film resistance, $R_s = 27\,\Omega$, for achieving good signal/noise ratio, while avoiding interference at high frequencies [19]. A Hewlett Packard/Agilent 33220A function generator applies a sinusoidal AC voltage with amplitude V_{ab} to the circuit (i. e., the voltage divider) and a Tektronix TDS 2002C two channel oscilloscope measures the voltages V_{ab} and V_{cb}. The oscilloscope bandwidth is 70 MHz, with DC vertical accuracy of $\pm(3\,\% \times \text{reading} + 0.1\,\text{div} + 1\,\text{mV})$, and delta time accuracy equal to $\pm(1\,\text{sample interval} + 100\,\text{ppm} \times \text{reading} + 0.6\,\text{ns})$.

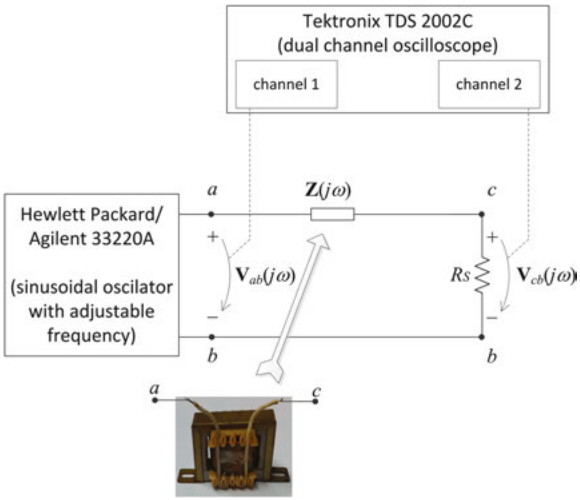

Figure 11: Experimental set-up EIS for measuring $Z(j\omega)$.

The tested inductor has a closed iron core, a resistance $R = 0.6\,\Omega$, measured by a Keithley 2000 digital multimeter by means of the 4-wire method, and an inductance $L = 11.5\,\text{mH}$, measured with a Escort ELC-131D LCR bridge at the frequency of 120 Hz. The experiments consist of measurements with linearly spaced exciting voltages $V_{ab} = \{1, \ldots, 10\}$ V. For each fixed-amplitude V_{ab}, the impedance $Z(j\omega)$ is obtained for the frequency range $2\pi \cdot 10 \leq \omega \leq 2\pi \cdot 10^4$ rad/s, at $K = 27$ logarithmically spaced points using the expression:

$$Z(j\omega) = R_s \cdot \left(\frac{V_{ab}(j\omega)}{V_{cb}(j\omega)} - 1 \right), \tag{52}$$

where the signals $v_{ab}(t) = V_{ab} \cos(\omega t)$ and $v_{cb}(t) = V_{cb} \cos(\omega t + \theta)$ are measured directly by the oscilloscope, and θ denotes the phase shift between $v_{cb}(t)$ and $v_{ab}(t)$.

In the follow-up we shall denote by Z_A and Z_R the impedances corresponding to the measured values and the reference (approximation) model, respectively.

The FO description is fitted into the data by minimizing the Canberra distance, J, between Z_A and Z_R, according with the expression:

$$J = \frac{1}{K} \sum_{k=1}^{K} \left(\frac{|\Re[Z_A(j\omega_k)] - \Re[Z_R(j\omega_k)]|}{|\Re[Z_A(j\omega_k)]| + |\Re[Z_R(j\omega_k)]|} + \frac{|\Im[Z_A(j\omega_k)] - \Im[Z_R(j\omega_k)]|}{|\Im[Z_A(j\omega_k)]| + |\Im[Z_R(j\omega_k)]|} \right), \tag{53}$$

where K is the total number of measuring points, as defined previously.

Expression (53) captures the relative error of the curve fitting. This avoids saturation effects that occur when using the standard Euclidean norm due to the simultaneous presence of large and small values.

A good fit occurs for the 5-parameter reference model:

$$Z_R(j\omega) = Z_0 \cdot \frac{(1 + \frac{j\omega}{z})^{\beta}}{(1 + \frac{j\omega}{p})^{\alpha}}, \tag{54}$$

where $Z_0 = 0.6$ is the inductor resistance measured in DC. Expression (54) represents a compromise between model complexity and quality of fitting between experimental and analytical results.

The polar, Nichols and Bode diagrams of $Z_A(j\omega)$ and $Z_R(j\omega)$ are depicted in Figure 12 for the excitation voltage $V_{ab} = 5$ V. The charts reveal the adequacy of expression (54) when modeling the inductor. For the other values of V_{ab}, the results are identical.

Table 2 summarizes the values of the parameters and the fitness function obtained for the 10 excitation voltages $V_{ab} = \{1, \ldots, 10\}$ V. We observe that the parameters z and p diminish for increasing values of the excitation voltage. On the other hand, α and β have a very small variation, revealing average and standard deviation values of $\{\mu_\alpha, \sigma_\alpha\} = \{0.536, 0.028\}$ and $\{\mu_\beta, \sigma_\beta\} = \{0.905, 0.025\}$, respectively. The fitness function, J, is minimal for intermediate values of V_{ab}, corresponding to a closer fit between $Z_A(j\omega)$ and $Z_R(j\omega)$.

Figure 13 depicts the Nichols diagrams of the inductor obtained with the experimental impedances, for $V_{ab} = \{1, \ldots, 10\}$ V. The points corresponding to the same frequency are also connected [13], so that we have the locus of constant frequency/amplitude versus variable amplitude/frequency. We observe that the impedance Z_A depends on V_{ab}, reflecting the nonlinear nature of the device. At low frequencies, Z_A is more

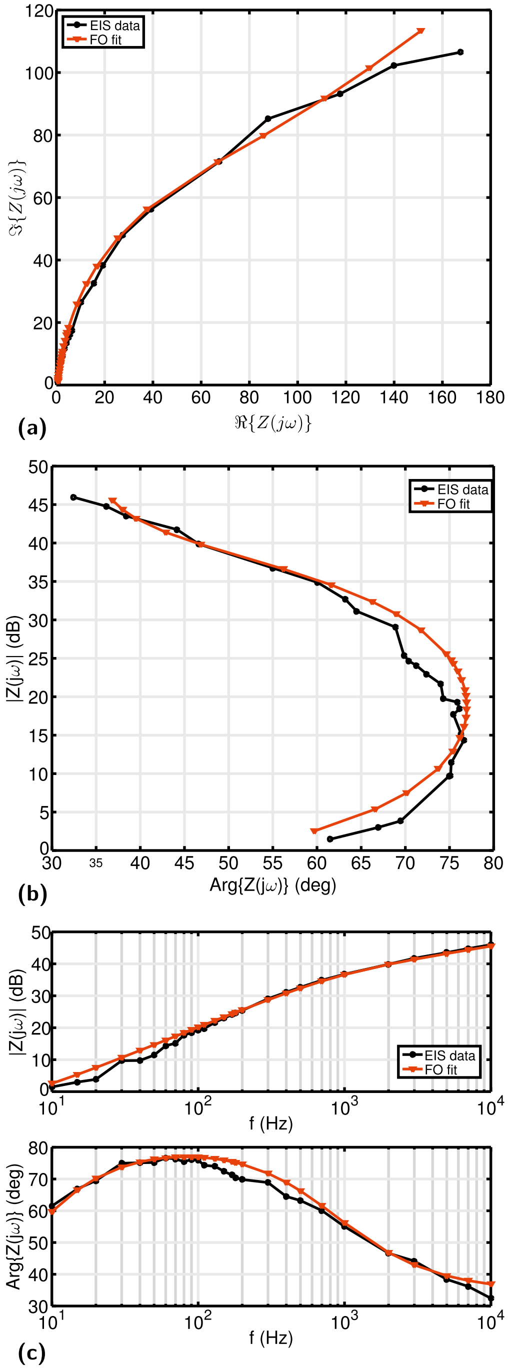

Figure 12: Diagrams of the experimental and model impedances, $Z_A(j\omega)$ and $Z_R(j\omega)$, of the inductor for $V_{ab} = 5$ V: (a) Polar; (b) Nichols; (c) Bode.

Table 2: Values of the parameters of the model and the fitness function for $V_{ab} = \{1, \ldots, 10\}$ V.

V_{ab}	z	β	p	α	J
1	38.96	0.92	8400	0.60	0.22
2	33.93	0.93	6200	0.55	0.16
3	32.67	0.92	6600	0.54	0.13
4	28.90	0.92	5100	0.54	0.11
5	28.90	0.92	5500	0.54	0.13
6	26.39	0.92	4800	0.54	0.10
7	22.62	0.90	4000	0.52	0.10
8	21.36	0.90	4000	0.52	0.14
9	16.34	0.86	4200	0.51	0.15
10	15.71	0.86	3900	0.50	0.20

sensitive to the excitation voltage, meaning that the nonlinear component represents a larger part of the total value.

The results demonstrate that model (54) yields a quantitative description and reliable characterization of the inductor. Nevertheless, the number of model parameters necessary is high and the adherence between the heuristic model and the experimental data in Figure 12 is limited.

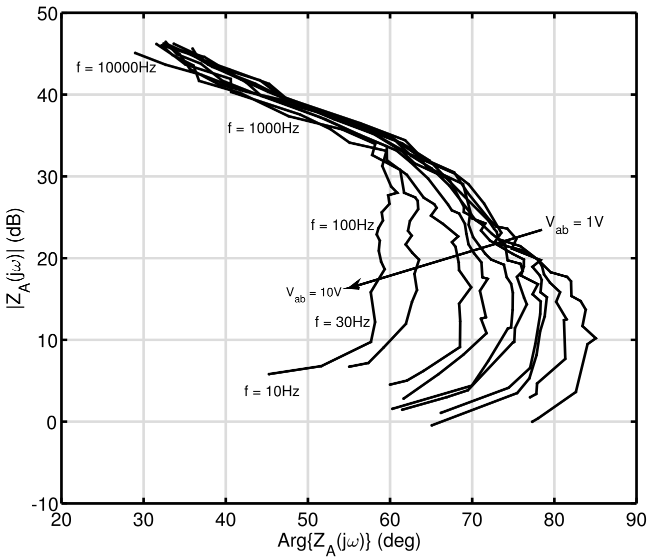

Figure 13: The Nichols diagrams of the inductor obtained with the experimental impedances, for $V_{ab} = \{1, \ldots, 10\}$ V.

6 Conclusion

This chapter presented four applications of FC in the area of electromagnetics, namely for modeling the electric potential generated by arbitrary charges, the electric transmission lines, the SE in an electric conductor, and the behavior of a nonlinear electric inductor. The phenomena and devices are well known and described by classic models. However, a closer look reveals that the FC formalism leads to a news perspective for evaluating more deeply all details. It was verified that the FO models characterize more accurately effects overlooked by standard approaches.

Bibliography

[1] M. Adachi, M. Sakamoto, J. Jiu, Y. Ogata, and S. Isoda, Determination of parameters of electron transport in dye-sensitized solar cells using electrochemical impedance spectroscopy, *J. Phys. Chem. B*, **110**(28) (2006), 13872–13880.

[2] R. B. Adler, L. J. Chu, and R. M. Fano, *Electromagnetic energy transmission and radiation*, Wiley, 1960.

[3] L. Bessonov, *Applied Electricity for Engineers*, MIR Publishers, Moscow, 1968.

[4] P. Bidan, Commande diffusive d'une machine electrique: une introduction, in *ESAIM Proceedings, France*, vol. 5, 1998.

[5] K. Biswas, G. Bohannan, R. Caponetto, A. Lopes, and J. A. T. Machado, *Fractional Order Devices*, Springer, 2017.

[6] A. Buscarino, R. Caponetto, G. Di Pasquale, L. Fortuna, S. Graziani, and A. Pollicino, Carbon black based capacitive fractional order element towards a new electronic device, *AEÜ, Int. J. Electron. Commun.*, **84** (2018), 307–312.

[7] M. Busłowicz, Stability analysis of continuous-time linear systems consisting of *n* subsystems with different fractional orders, *Bull. Pol. Acad. Sci., Tech. Sci.*, **60**(2) (2012), 279–284.

[8] S. Canat and J. Faucher, Fractional order: frequential parametric identification of the skin effect in the rotor bar of squirrel cage induction machine, in *ASME Design Engineering Technical Conferences 2003VIB-48393*, vol. 48393, 2003.

[9] S. H. Cha, Comprehensive survey on distance/similarity measures between probability density functions, *Int. J. Math. Models Methods Appl. Sci.*, **4** (2007), 300–307.

[10] R. A. Chipman, *Transmission Lines*, McGraw-Hill, 1968.

[11] K. S. Cole and R. H. Cole, Dispersion and absorption in dielectrics I. Alternating current characteristics, *J. Chem. Phys.*, **9**(4) (1941), 341–351.

[12] D. W. Davidson and R. H. Cole, Dielectric relaxation in glycerol, propylene glycol, and *n*-propanol, *J. Chem. Phys.*, **19**(12) (1951), 1484–1490.

[13] F. Duarte and J. A T. Machado, Describing function of two masses with backlash, *Nonlinear Dyn.*, **56**(4) (2009), 409–413.

[14] D. El Khaled, N. N. Castellano, J. A. Gazquez, R. M. García Salvador, and F. Manzano-Agugliaro, Cleaner quality control system using bioimpedance methods: A review for fruits and vegetables, *J. Clean. Prod.*, **140** (2017), 1749–1762.

[15] N. Engheta, On fractional calculus and fractional multipoles in electromagnetism, *IEEE Trans. Antennas Propag.*, **44**(4) (1996), 554–566.

[16] S. Ghasemi, M. T. Darestani, Z. Abdollahi, and V. G. Gomes, Online monitoring of emulsion polymerization using electrical impedance spectroscopy, *Polym. Int.*, **64**(1) (2015), 66–75.

[17] M. Glatthaar, M. Riede, N. Keegan, K. Sylvester-Hvid, B. Zimmermann, M. Niggemann, A. Hinsch, and A. Gombert, Efficiency limiting factors of organic bulk heterojunction solar cells identified by electrical impedance spectroscopy, *Sol. Energy Mater. Sol. Cells*, **91**(5) (2007), 390–393.

[18] F. Groeber, L. Engelhardt, S. Egger, H. Werthmann, M. Monaghan, H. Walles, and J. Hansmann, Impedance spectroscopy for the non-destructive evaluation of in vitro epidermal models, *Pharm. Res.*, **32**(5) (2015), 1845–1854.

[19] S. Guinta, Ask the applications engineer–resistors, *Analog Dialogue: A Forum for the Exchange of Circuits, Systems and Software for Real-World Signal Processing*, **31**(1) (1997), 1–24.

[20] S. Havriliak and S. Negami, A complex plane analysis of α-dispersions in some polymer systems, *J. Polym. Sci., C Polym. Symp.*, **14** (1966), 99–117.

[21] C. Ionescu, A. M. Lopes, D. Copot, J. A. T. Machado, and J. H. T. Bates, The role of fractional calculus in modeling biological phenomena: A review, *Commun. Nonlinear Sci. Numer. Simul.*, **51** (2017), 141–159.

[22] A. Jalloul, J.-C. Trigeassou, K. Jelassi, and P. Melchior, Fractional order modeling of rotor skin effect in induction machines, *Nonlinear Dyn.*, **73**(1–2) (2013), 801–813.

[23] I. S. Jesus and J. A. T. Machado, Implementation of fractional-order electromagnetic potential through a genetic algorithm, *Commun. Nonlinear Sci. Numer. Simul.*, **14**(5) (2009), 1838–1843.

[24] Á. Kertész, Z. Hlaváčová, E. Vozáry, and L. Staroňová, Relationship between moisture content and electrical impedance of carrot slices during drying, *Int. Agrophys.*, **29**(1) (2015), 61–66.

[25] M. S. Krishna, S. Das, K. Biswas, and B. Goswami, Fabrication of a fractional order capacitor with desired specifications: a study on process identification and characterization, *IEEE Trans. Electron Devices*, **58**(11) (2011), 4067–4073.

[26] K. Küpfmüller, *Einführung in die Theoretische Elektrotechnik*, Springer-Verlag, Berlin, 1939.

[27] R. B. Leighton, R. P. Feynman, and M. Sands, *The Feynman Lectures on Physics: Mainly Electromagnetism and Matter*, Addison-Wesley Pub. Company, Reading, Massachusetts, 1964.

[28] M. Lewandowski and M. Orzyłowski, Fractional-order models: The case study of the supercapacitor capacitance measurement, *Bull. Pol. Acad. Sci., Tech. Sci.*, **65**(4) (2017), 449–457.

[29] A. Lopes and J. A. T. Machado, Fractional order models of leaves, *J. Vib. Control*, **20**(7) (2014), 998–1008.

[30] A. Lopes and J. A. T. Machado, Modeling vegetable fractals by means of fractional-order equations, *J. Vib. Control*, **22**(8) (2016), 2100–2108.

[31] A. Lopes and J. A. T. Machado, Fractional-order model of a non-linear inductor, 2018, in press.

[32] A. Lopes, J. A. T. Machado, and E. Ramalho, On the fractional-order modeling of wine, *Eur. Food Res. Technol.*, **243**(6) (2017), 921–929.

[33] A. Lopes, J. A. T. Machado, E. Ramalho, and V. Silva, Milk characterization using electrical impedance spectroscopy and fractional models, in *Food Analytical Methods*, pp. 1–12, 2017.

[34] J. A. T. Machado and A. Galhano, Generalized two-port elements, *Commun. Nonlinear Sci. Numer. Simul.*, **42** (2017), 451–455.

[35] J. A. T. Machado and I. S. Jesus, A suggestion from the past? *Fract. Calc. Appl. Anal.*, **7**(4) (2004), 403–407.

[36] J. A. T. Machado and A. Lopes, The persistence of memory, *Nonlinear Dyn.*, **79**(1) (2015), 63–82.

[37] J. A. T. Machado M. W. Albert, J. Fernando Silva, and M. T. Correia de Barros, Fractional order calculus on the estimation of short-circuit impedance of power transformers, in *Proc. 1st IFAC Workshop on Fractional Differentiation and Its Applications, Bordeaux, France*, 2004.

[38] J. A. T. Machado, I. S. Jesus, A. Galhano, and J. B. Cunha, Fractional order electromagnetics, *Signal Process.*, **86**(10) (2006), 2637–2644.

[39] J. A. T. Machado, I. S. Jesus, A. Galhano, J. B. Cunha, and J. K. Tar, Fractional calculus analysis of the electrical skin phenomena, in O. P. Agrawal, J. Sabatier, and J. A. T. Machado (eds.), *Advances in Fractional Calculus: Theoretical Developments and Applications in Physics and Engineering*, pp. 323–332, Springer, Dordrecht, The Netherlands, 2007.

[40] J. A. T. Machado, A. Galhano, A. Oliveira, and J. K. Tar, Optimal approximation of fractional derivatives through discrete-time fractions using genetic algorithms, *Commun. Nonlinear Sci. Numer. Simul.*, **15**(3) (2010), 482–490.

[41] J. A. T. Machado, A. Lopes, F. Duarte, M. Ortigueira, and R. Rato, Rhapsody in fractional, *Fract. Calc. Appl. Anal.*, **17**(4) (2014), 1188–1214.

[42] P. Melchior, B. Orsoni, O. Lavialle, A. Poty, and A. Oustaloup, Consideration of obstacle danger level in path planning using A* and Fast-Marching optimisation: comparative study, *Signal Process.*, **83**(11) (2003), 2387–2396.

[43] A. Milton and I. A. Stegun, *Handbook of Mathematical Functions with Formulas, Graphs, and Mathematical Tables*, Dover Pub. Inc., New York, 1965.

[44] T. Poinot, A. Benchellal, S. Bachir, and J.-C. Trigeassou, Identification of a non-integer model of induction machines, in *Proc.1st IFAC Workshop on Fractional Differentiation and Its Applications, Bordeaux, France*, 2004.

[45] S. Racewicz, Identification and non-integer order modelling of synchronous machines operating as generator, *Acta Energ.*, 2012.

[46] H. Samavati, A. Hajimiri, A. R. Shahani, G. N. Nasserbakht, and T. H. Lee, Fractal capacitors, *IEEE J. Solid-State Circuits*, **33**(12) (1998), 2035–2041.

[47] I. Schäfer and K. Krüger, Modelling of coils using fractional derivatives, *J. Magn. Magn. Mater.*, **307**(1) (2006), 91–98.

[48] I. Schäfer and K. Krüger, Modelling of lossy coils using fractional derivatives, *J. Phys. D, Appl. Phys.*, **41**(4) (2008), 045001.

[49] V. E. Tarasov, Review of some promising fractional physical models, *Int. J. Mod. Phys. B*, **27**(09) (2013), 1330005.

[50] A. R. West, D. C. Sinclair, and N. Hirose, Characterization of electrical materials, especially ferroelectrics, by impedance spectroscopy, *J. Electroceram.*, **1**(1) (1997), 65–71.

[51] S. Westerlund, Dead matter has memory! *Phys. Scr.*, **43**(2) (1991), 174.

Vasily E. Tarasov
Fractional electrodynamics with spatial dispersion

Abstract: Nonlocal electrodynamics of media with power-law spatial dispersion (PLSD) are described. Spatial dispersion is a phenomenon in which the absolute permittivity of the media depends on the wave vector. Power-law spatial dispersion is described by derivatives and integrals of noninteger orders. Fractional differential equations for the electric fields in these media are suggested. The generalizations of Coulomb's law and Debye's screening for power-law nonlocal media are proposed. Simple models of anomalous behavior of media with PLSD are described as nonlocal properties of power-law type. As examples, we consider electric fields of point charge and dipole in media with PLSD, infinite charged wire, uniformly charged disk, capacitance of spherical capacitor, and multipole expansion for media with PLSD. A microscopic model, which is based on fractional kinetics, is proposed to describe spatial dispersion of power-law type. The fractional Liouville equation is used to obtain the power-law dependence of the absolute permittivity on the wave vector. The proposed fractional nonlocal electrodynamics is characterized by universal spatial behavior of electromagnetic fields in media with PLSD by analogy with the universal temporal behavior of low-loss dielectrics.

Keywords: Spatial dispersion, electrodynamics, fractional calculus, fractional Laplacian, Riesz potential

PACS: 03.50.De, 45.10.Hj, 41.20.-q, 05.20.-y, 51.10.+y

1 Introduction

Spatial dispersion is a phenomenon of the dependence of the absolute permittivity tensor of the medium on the wave vector [28, 7, 5]. This dependence leads to different effects, including the rotation of the plane of polarization, anisotropy of cubic crystals and others [4, 3, 2, 6, 17, 18, 12, 26, 10, 11, 8, 1]. The spatial dispersion is caused by nonlocal connection between the electric induction $\mathbf{D}$ and the electric field $\mathbf{E}$. Vector $\mathbf{D}$ at any point $\mathbf{r}$ of the medium is not uniquely defined by the values of $\mathbf{E}$ at this point. It also depends on the values of $\mathbf{E}$ at neighboring points $\mathbf{r}'$.

Media with high spatial dispersion are called plasma-like media. The term "plasma-like media" was proposed by Viktor P. Silin and Henri A. Rukhadze in 1961 in book [28]. Plasma-like medium is medium, in which the motion of free charge carriers cre-

Vasily E. Tarasov, Skobeltsyn Institute of Nuclear Physics, Lomonosov Moscow State University, Moscow 119991, Russia, e-mail: tarasov@theory.sinp.msu.ru

https://doi.org/10.1515/9783110571721-002